IEEE Access
Multidisciplinary ⋮ Rapid Review ⋮ Open Access Journal

Received March 8, 2020, accepted April 17, 2020, date of publication April 22, 2020, date of current version May 8, 2020.

Digital Object Identifier 10.1109/ACCESS.2020.2989581

Dual-Band Dual-Linear Polarization Reflectarray for mmWaves/5G Applications

SANDRA COSTANZO, (Senior Member, IEEE), FRANCESCA VENNERI, (Member, IEEE), ANTONIO BORGIA, (Member, IEEE), AND GIUSEPPE DI MASSA, (Life Senior Member, IEEE)
Università della Calabria, 87036 Rende, Italy

Corresponding author: Sandra Costanzo (costanzo@dimes.unical.it)

ABSTRACT A dual-band dual-linear polarization reflectarray configuration is developed for future 5G cellular applications. A single layer unit cell including two pairs of miniaturized fractal patches is designed to operate at two distinct frequencies within the Ka-band (27/32 GHz), in a dual-polarization mode. An in-depth analysis of the unit cell behavior is carried out, to demonstrate the total independence between the designed frequency bands and polarizations. The proposed configuration offers a very simply and thin structure, small unit cell sizes, and low losses, while leading to an independent optimization of the phase at each frequency and polarization. A dual-band/dual-polarized reflectarray prototype is designed and tested, thus demonstrating the unit cell flexibility to offer arbitrary beam directions/shapes at each frequency, for both polarizations.

INDEX TERMS Reflectarray, dual-band, dual-polarization, 5G, millimeter waves.

I. INTRODUCTION

Currently, the international telecommunication scientific community is focused on the development of the enabling technologies for next generation 5G communication systems. 5G wireless communication networks are expected to meet the growing demand for higher data rates (i.e. 1-10 Gbps), lower network latencies, and better energy efficiency [1]. To address these demands, 5G systems will use millimeter wave (mmw) frequencies, which represent one of the key enabling technologies in the implementation of 5G networks. As a matter of the fact, the unlicensed/underutilized mmw frequency bands provide great amount of available spectrum resources that can support the requirements for high data rate and low latency [1]–[3]. Conversely, mmw technology requires high gain antenna systems [4]–[6] to compensate for the intrinsic higher path loss, mainly due to the atmospheric absorption of electromagnetic waves at higher frequencies. To this end, microstrip reflectarrays could represent a very attractive solution for designing high gain antennas for 5G systems [7], [8]. As well known, microstrip reflectarrays consist of an array of printed radiators illuminated by a feed antenna. Each element in the array is designed to introduce a proper phase delay in the re-radiated field component, giving an overall radiation pattern with a prescribed beam direction and/or shape [7]–[12]. Reflectarrays can provide very high efficiencies, due to the adopted spatial feeding approach [7]. Furthermore, they offer several reconfiguration capabilities, such as beam-steering [7], [13]–[17], multi-beam radiation patterns [7], [13], multi-band functions and/or polarization diversity [19]–[23].

In this paper, the design of a single layer dual-band/dual-polarized reflectarray cell is discussed. The proposed unit cell consists of four miniaturized fractal-based elements printed on a grounded dielectric substrate. The patches are grouped into two pairs, each one operating at two distinct frequencies within the Ka-band (i.e. 27 and 32 GHz). The single pair is composed of two linearly polarized patches, which are rotated 90 degrees with respect to each other, thus realizing the double polarization operation at both frequencies. The reflection phase can be separately adjusted, in correspondence of each frequency/polarization, by independently varying a proper defined scaling factor for each element. The same concept has already been adopted by the authors in [24] to design a dual-band (28/38 GHz) reflectarray unit cell. Furthermore, a preliminary investigation of the proposed cell has been illustrated in [25]. Unlike existing multiband and/or dual polarized reflectarray configurations, the proposed reflectarray cell allows to achieve the following benefits: a simpler and thinner structure ($h \cong 0.027\lambda$ @ the upper frequency) with respect to the most multilayer stacked configurations [19, 20]; smaller unit cell sizes at both operating frequencies ($\cong 0.49\lambda$

The associate editor coordinating the review of this manuscript and approving it for publication was Irfan Ahmed.

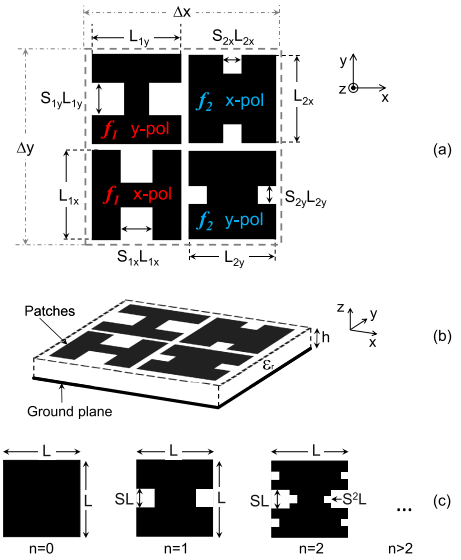

FIGURE 1. Dual-band/dual-polarized reflectarray unit cell: (a) top view; (b) 3D view and stratification; (c) fractal construction.

@ 27 GHz, ≅ 0.58λ @ 32 GHz) with respect to other single-layer configurations [21, 22], thus preserving the capability to point the main beam at large scan angles; small electrical interferences between the elements operating at the two different bands, despite the adopted small inter-element spacing. As a proof of concept, the designed unit cell is adopted to synthesize a reflectarray having arbitrary beam directions at each frequency and polarization. The experimental validation of the designed prototype confirms the effectivness of the proposed dual-band/dual-polarized reflectarray cell. Due to its compactness and versatility, the proposed dual-band/dual polarized reflectarray cell is very appealing for future 5G applications. As a matter of the fact, the implementation of compact antennas offering multi-band operation and polarization diversity could be very useful to increase 5G network capacity [1]–[3], [23].

II. UNIT CELL LAYOUT AND DESIGN

The proposed dual-band/dual-polarized reflectarray cell is composed by two pairs of miniaturized patches printed on the same substrate layer (Fig. 1). Each pair operates at a specific resonant frequency (i.e. f_1 and f_2 - see Fig.1(a)). Two linearly polarized elements are assumed, which are rotated each other by 90 degrees, thus offering a dual polarization operation mode (i.e. x/y-polarized - see Fig.1(a)) at both frequencies. The layout of the single patch embedded into the cell is derived from the 1st iteration fixed-length fractal patch (Fig. 1(c)), proposed by the authors in [26], [27]. The element is characterized by a beginning square patch of dimensions $L_{fp} \times L_{fp}$ ($f = 1, 2$; $p = x, y$ in Fig. 1(a)). A smaller ($S_{fp}L_{fp} \times S_{fp}L_{fp}$)-square is removed from the center of both resonant sides of the beginning patch. S_{fp} is the fractal-scaling factor that may vary from 0 up to 0.45. The reflection phase tuning is realized by independently varying the fractal scaling factors S_{fp}, leaving unchanged the patches size $L_{fp} \times L_{fp}$.

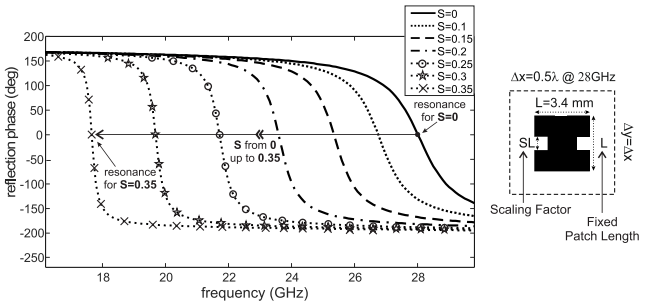

FIGURE 2. Simulated phase curves vs frequency for different values of the scaling factor S (L = 3.4mm, Δx × Δy = 0.5λ × 0.5λ @28 GHz).

A. MINIATURIZATION SKILLS OF THE PROPOSED FRACTAL PATCHES

As demonstrated in [26]–[29], the main benefit of fractal geometries is that a greater electrical length can be fitted into a smaller physical area; namely, the fractal metallic patch should be miniaturized in order to obtain the resonance at the desired operating frequency.

The adopted fractal shape (Fig. 1(c)), for example, allows to achieve an appreciable reduction in size (up to 50%) with respect to the standard square patch. As depicted in Fig. 2, illustrating the simulated reflection phase of a 1st iteration fractal patch, printed on a Diclad880 substrate ($\varepsilon_r = 2.24$, h = 0.254mm), an increasingly smaller resonant frequency is obtained by progressively increasing the scaling factor S from 0 up to 0.35, for a fixed value of the patch length.

In particular, the resonance frequency moves from the square patch resonant value of 28 GHz down to 17.5 GHz (S = 0.35), which is equivalent to a 37.5% size reduction. This latter behavior demonstrates the high miniaturization capability of the proposed fractal element, which becomes more relevant when a greater value of the scaling factor S is considered (Fig. 2) and/or the fractal construction is progressively reiterated [27]. However, the feasibility of the proposed configuration, especially for reiterated fractal construction, can be guaranteed up to a certain frequency (≤50÷55GHz), which is correlated to the substrate features as well as to the accuracy of the adopted fabrication process [30].

B. DESIGN OF A DUAL-BAND/DUAL-POLARIZED REFLECTARRAY CELL

The miniaturization skills of the proposed fractal patch [26] allow to obtain a dual-band/dual-polarization behavior, by simply embedding four miniaturized elements within the same unit cell, while preserving, at the same time, the compactness of the array grid (Δx, Δy <0.6λ) and the independence between the designed frequency bands and polarizations. The layout depicted in Fig. 1(a) is adopted to design a dual-band unit cell operating at the following frequencies: $f_1 = 27$ GHz and $f_2 = 32$ GHz, in a dual-linear polarization mode. The above frequencies are chosen because they fall into the new 5G cellular bands, which are under consideration at the International Telecommunications Union's (ITU) World Radiocommunication Conference

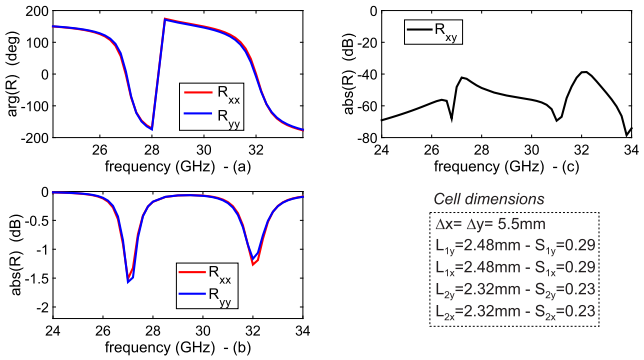

FIGURE 3. Reflection coefficient vs frequency: (a) phase for each polarization; (b) magnitude for each polarization; (c) magnitude of the cross-polar components.

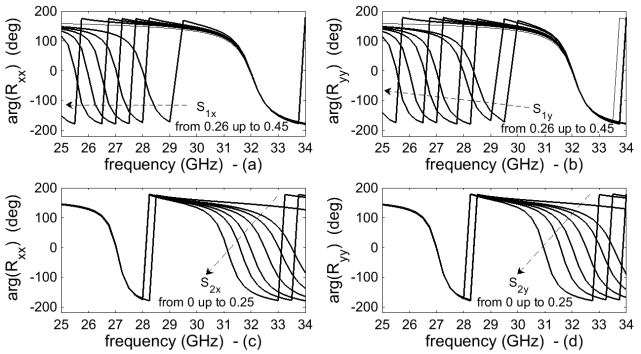

FIGURE 4. Reflection phase vs frequency for different values of the scaling factors S_{fp}: (a) S_{1x} variable, S_{1y}, S_{2x}, S_{2y} fixed (i.e. phase response due to the x-polarized 27GHz-patch); (b) S_{1y} variable, S_{1x}, S_{2x}, S_{2y} fixed (i.e. phase response due to the y-polarized 27GHz-patch); (c) S_{2x} variable, S_{1x}, S_{1y}, S_{2y} fixed (i.e. phase response due to the x-polarized 32GHz-patch); (d) S_{2y} variable, S_{1x}, S_{1y}, S_{2x} fixed (i.e. phase response due to the y-polarized 32GHz-patch).

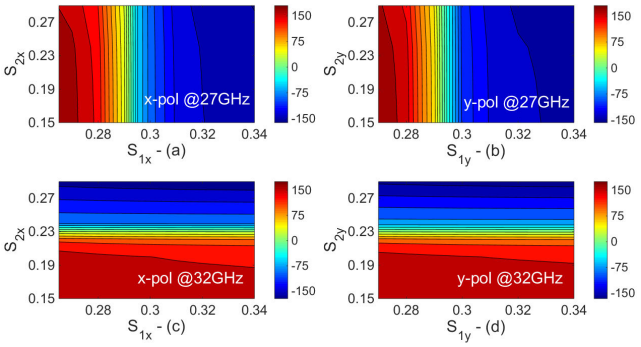

FIGURE 5. Reflection phase computed for different polarizations and frequencies - Normal incidence (θ_{inc}, ϕ_{inc}) = (0°,0°): (a) phase response due to the x-polarized 27GHz-patch vs S_{1x} and S_{2x}; (b) phase response due to the y-polarized 27GHz-patch vs S_{1y} and S_{2y}; (c) phase response due to the x-polarized 32GHz-patch vs S_{1x} and S_{2x}; (d) phase response due to the y-polarized 32GHz-patch vs S_{1y} and S_{2y}.

(WRC-19) [31]. Greater frequency ratios (f_2/f_1) can be synthesized through the use of the proposed dual-band fractal cell [24], by properly choosing the fractal dimensions, L_{fp} and S_{fp}. As a matter of the fact, the operating frequency of each pair of patches is inversely proportional to the effective side lengths, $L_{fp}^{eff} = (1 + S_{fp})L_{fp}$, so the longer the effective fractal side is, the smaller the resonant frequency will be and vice versa. Then, the achievable (f_2/f_1)-ratio depends on the following parameters: the maximum L_{fp}-values imposed by the unit cell size, $\Delta x \times \Delta y$; the maximum frequency value (i.e. f_2) due to the actual feasibility of the fractal-structure (see Section II.A).

In the example presented in this work, a Diclad880 dielectric substrate, having $\varepsilon_r = 2.24$ and $h = 0.254$mm (Fig. 1(b)), is considered. A commercial full-wave code is adopted as analysis tool, imposing the infinite periodic array conditions [32]. A normal incident plane wave is applied. A periodicity equal to $\Delta x = \Delta y = 5.5$ mm is fixed, corresponding to 0.49λ at 27 GHz and 0.58λ at 32 GHz.

Taking into account the fractal patch behavior illustrated in Fig. 2 and following the design rules outlined in [26], the desired dual-resonant/dual-polarization unit cell is synthesized, by fixing the patches dimensions (i.e. L_{fp} and S_{fp}) to the values reported in Fig. 3. As a matter of the fact, a dual resonant behavior can be observed in the unit cell reflection phase and amplitude (i.e. arg(R) in Fig. 3(a) and abs(R) in Fig. 3(b)), computed both in the case of an x-polarized incident wave (see R_{xx}) as well as in the case of a y-polarized one (see R_{yy}). Furthermore, Fig. 3(c) shows very low cross-polarization levels (i.e. R_{xy}) at both frequencies (< -38dB).

As depicted in Fig. 4, a negligible mutual coupling between the two bands is obtained for both polarizations, assuring an independent phase tuning mechanism for each frequency/polarization, by simply changing the corresponding scaling factors (i.e. S_{1x} for $f_1 = 27$ GHz / x-polarization; S_{1y} for $f_1 = 27$ GHz / y-polarization; S_{2x} for $f_2 = 32$ GHz / x-polarization; S_{2y} for $f_2 = 32$ GHz / y-polarization), within the values ranges reported in Fig. 4.

In order to give a more exhaustive description of the designed dual-band/dual polarized unit cell, Fig. 5 illustrates the variations in phase of the coefficients R_{xx} and R_{yy}, at 27 GHz (Fig. 5(a, b)) and 32 GHz (Fig. 5(c, d)), with respect to the scaling factors of the patches polarized in the corresponding directions.

As it can be observed, the phase response at 27 GHz can be completely controlled by the scaling factors S_{1x} and S_{1y}, while the phase response at 32 GHz can be independently tuned by varying the scaling factors S_{2x} and S_{2y}. As a matter of the fact, a quite constant reflection phase can be observed @ 27 GHz (Fig. 5(a, b)), by changing the scaling factors S_{2p} ($p = x, y$ in Fig. 1(a)) for a fixed S_{1p}-value (Fig. 3). Similar considerations can be extrapolated from Fig. 5(c, d) at the frequency $f_2 = 32$ GHz.

Furthermore, Fig. 6 shows the polarizations independence of the cell at both frequencies. As a matter of the fact, a quite constant reflection phase can be observed @ 27 GHz (Fig. 6(a, b)), by changing the scaling factors S_{1y} for a fixed S_{1x}-value (Fig. 6(a)) and vice versa (Fig. 6(b)). Similar considerations can be extrapolated from Fig. 6(c, d) at the frequency $f_2 = 32$ GHz.

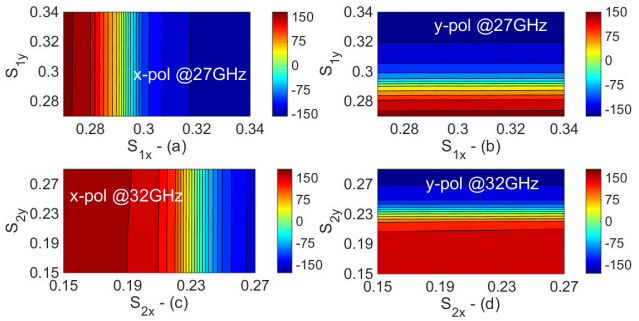

FIGURE 6. Reflection phase computed for different polarizations and frequencies - Normal incidence (θ_{inc}, ϕ_{inc}) = (0°,0°): (a) phase response due to the x-polarized 27GHz-patch vs S_{1x} and S_{1y}; (b) phase response due to the y-polarized 27GHz-patch vs S_{1x} and S_{1y}; (c) phase response due to the x-polarized 32GHz-patch vs S_{2x} and S_{2y}; (d) phase response due to the y-polarized 32GHz-patch vs S_{2x} and S_{2y}.

TABLE 1. Comparison of unit cell sizes and thickness.

Unit Cell	Cell stratification	f_1 [GHz]	f_2 [GHz]	Cell sizes	Cell thickness
Proposed configuration	Single layer	27	32	$0.58\lambda@f_2$	$0.027\lambda@f_2$
[19]	Multi-layer	12	19.5	$0.65\lambda@f_2$	$0.25\lambda@f_2$
[20]	Multi-layer	10	15	$0.46\lambda@f_2$	$0.21\lambda@f_2$
[21]	Single layer	8.2	13.2	$0.75\lambda@f_2$	$0.3\lambda@f_2$
[22]	Single layer	10.2	22	$0.63\lambda@f_2$	$0.1@f_2$

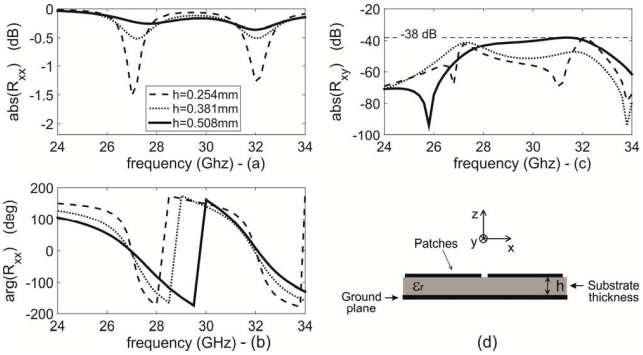

FIGURE 7. Reflection coefficient vs frequency for different substrate thickness: (a) amplitude; (b) phase; (c) unit cell side view and stackup.

Finally, Table 2 shows the main structural benefits offered by the proposed cell, with respect to the existing multiband and/or dual polarized reflectarray configurations. In particular, a thinner profile can be observed, compared to the most multilayer stacked configurations [19], [20], while smaller unit cell sizes are achieved with respect to the other single-layer configurations [21], [22].

C. PARAMETRIC ANALYSIS OF THE PROPOSED UNIT CELL

In order to give a more comprehensive characterization of the proposed dual-band/dual-polarized unit cell, a parametric analysis of reflection coefficient behavior is performed, by varying the substrate thickness and the incident angle of the impinging plane wave.

Fig. 7 illustrates the unit cell reflection coefficient vs frequency, computed in the case of an x-polarized incident wave, for different substrate thicknesses. Table 2 shows the

TABLE 2. Unit cell sizes for different substrate thicknesses.

h [mm]	L_{1x}[mm] (S_{1x})	L_{1y}[mm] (S_{1y})	L_{2x}[mm] (S_{2x})	L_{2y}[mm] (S_{2y})
0.254	2.48 (0.29)	2.48 (0.29)	2.32 (0.23)	2.32 (0.23)
0.381	2.49 (0.28)	2.48 (0.28)	2.31 (0.21)	2.32 (0.21)
0.508	2.44 (0.28)	2.41 (0.28)	2.23 (0.21)	2.24 (0.22)

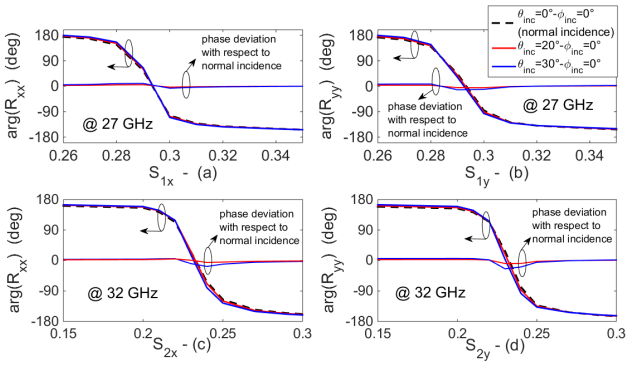

FIGURE 8. Reflection coefficient vs. elements scaling factor for different values of incidence angle θ_{inc} (plane $\phi_{inc} = 0°$): (a) vs S_{1x} @27 GHz; (b) vs S_{1y} @27 GHz; (c) vs S_{2x} @32 GHz; (d) vs S_{2y} @32 GHz.

dimensions of the synthesized unit cells that are respectively printed on a substrate layer with a thickness-value ranging from 0.254 mm (≅ 0.027λ @ 32GHz) up to 0.508 mm (≅ 0.054λ @ 32GHz). As it is well known, the use of a thicker substrate allows to reduce the reflection losses, that vary from −1.5 dB down to −0.36 dB. Furthermore, smoother phase curves can be achieved, giving improved bandwidth performances. In this regards, it is important to stress how the substrate thicknesses remain very small compared to the multilayer dual-band unit cells proposed in the literature [19], [20]. Furthermore, very low cross-polarization levels (abs(R_{xy}) < −38dB) are obtained at both frequencies, in the case of normal incidence. Similar results are achieved when a y-polarized plane wave is considered as source.

However, as it can be guessed from Fig. 7(b), the achievable phase range vs the scaling factors S_{np} becomes smaller when the substrate thickness increases (in the case of the cells considered in Table 2, for example, the phase range results to be equal to 340° for h = 0.254mm, 325° for h = 0.381mm and 305° for h = 0.508mm). For the above reasons, it is essential to find the right tradeoff between unit cell phase ranges, losses and bandwidth, during the synthesis stage of the reflectarray cell.

Finally, the reflection phase of the synthesized cell is computed by assuming an oblique incident plane wave, for both polarizations. Figs. 8 and 9 show acceptable phase variations under 20° and 30° oblique incidences, as compared to the normal case, both in the principal plane, $\phi = 0°$ (Fig. 8), as well as in the ($\phi = 30°$)-plane (Fig. 9). As a matter of the fact, very similar phase curves can be observed, at both operating frequencies and for both polarizations, with a maximum phase error less or equal to 20°. Furthermore, a quite

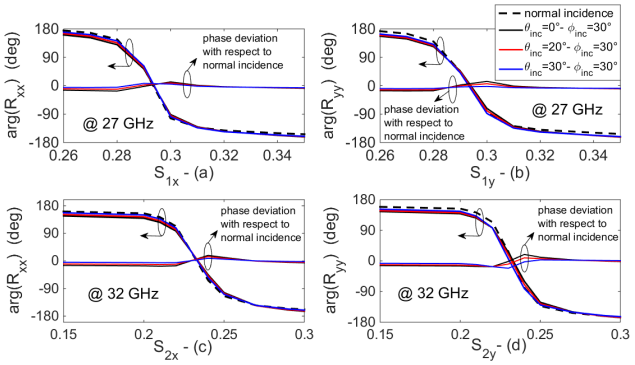

FIGURE 9. Reflection coefficient vs. elements scaling factor for different values of incidence angle θ_{inc}(plane $\phi_{inc} = 30°$): (a) vs S_{1x} @27 GHz; (b) vs S_{1y} @27 GHz; (c) vs S_{2x} @32 GHz; (d) vs S_{2y} @32 GHz.

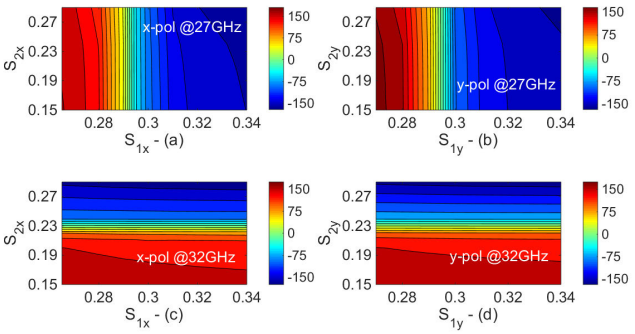

FIGURE 10. Reflection phase computed for different polarizations and frequencies - Oblique incidence (θ_{inc}, ϕ_{inc}) = (30°,30°): (a) phase response due to the x-polarized 27GHz-patch vs S_{1x} and S_{2x}; (b) phase response due to the y-polarized 27GHz-patch vs S_{1y} and S_{2y}; (c) phase response due to the x-polarized 32GHz-patch vs S_{1x} and S_{2x}; (d) phase response due to the y-polarized 32GHz-patch vs S_{1y} and S_{2y}.

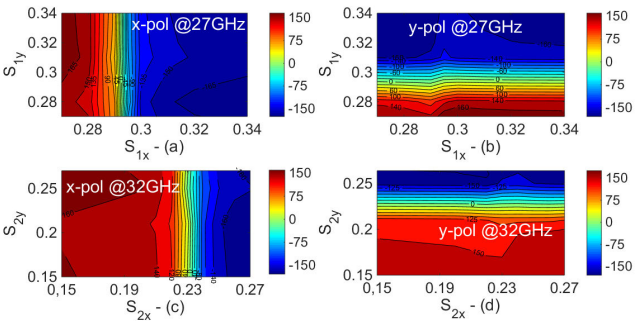

FIGURE 11. Reflection phase computed for different polarizations and frequencies - Oblique incidence (θ_{inc}, ϕ_{inc}) = (30°,30°): (a) phase response due to the x-polarized 27GHz-patch vs S_{1x} and S_{1y}; (b) phase response due to the y-polarized 27GHz-patch vs S_{1x} and S_{1y}; (c) phase response due to the x-polarized 32GHz-patch vs S_{2x} and S_{2y}; (d) phase response due to the y-polarized 32GHz-patch vs S_{2x} and S_{2y}.

good polarizations independence at both frequencies is also demonstrated for the case of an oblique incident plane wave (Figs. 10 and 11). In particular, Figs. 10 and 11 illustrate the unit cell reflection phase behavior out of the principal planes, namely for an incident direction equal to (θ_{inc}, ϕ_{inc}) = (30°, 30°). A similar behavior can be observed in the unit cell phase response with respect to those achieved in the case of normal incidence (Figs. 5 and 6), with a maximum phase deviation of about 25°, which can be considered quite acceptable. Finally,

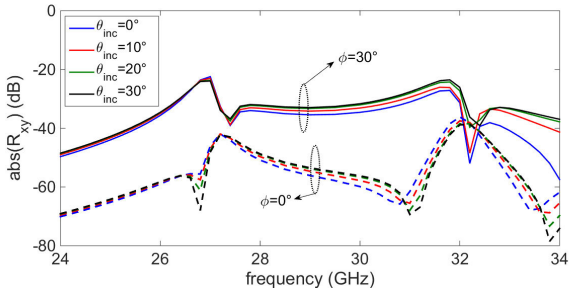

FIGURE 12. Magnitude of the cross-polar component R_{xy} for different incident angles.

Fig. 12 shows the cross polarization level of the cell for different incident angles. In particular, it can be observed that the cross-polarization increases in the ($\phi = 30°$)-plane, but still remaining considerably lower than -23dB. Conversely, negligible variations can be observed in the unit cell cross-polarized components, for different values of the incident angle θ_{inc}. The above analysis leads to consider the proposed configuration quite independent on the angle of incidence.

III. NUMERICAL VALIDATION OF A DUAL-BAND DUAL-LINEAR POLARIZATION REFLECTARRAY

The proposed dual-band/dual-polarized unit cell is adopted to design two reflectarrays operating within the Ka-band, which is under consideration for 5G. The low mutual coupling between the two designed frequency bands and polarizations, allows to separately synthesize four sets of miniaturized patches (each identified by L_{1x}, L_{1y}, L_{2x} and L_{2y} - see Fig.1). A synthesis algorithm, based on the iterative projection method [33], is applied to compute the crucial phase distribution on each of the four elements embedded into the (n,m)-array cells. A set of upper- and lower-bound masks [33] is properly defined, imposing the desired constraints on the patterns radiated at each considered frequency and polarization. The implemented synthesis algorithm returns four sets of phase coefficients ϕ_{fp}(n,m) to be imposed on the (n,m)-reflectarray cells. These last data are finally adopted to select the scaling factors S_{fp}(n,m) of each of the four elements embedded into the (n,m) reflectarray cells, by using the computed design curves depicted in Fig. 4. To this end, a research routine is defined that fits the desired ϕ_{fp}(n,m) values onto the simulated phase curves, finally returning the corresponding scaling factors S_{fp}(n,m). More details on the adopted research routine are reported in [13], [33].

In the following sections, two different reflectarray designs are illustrated. The first one (Design #1- Section A) aims to prove the versatility of the proposed configuration in achieving arbitrary beam directions/shapes at each frequency and polarization. For the sake of simplicity, a normally impinging plane wave is considered as source, thus neglecting the effect of a real feed. The second example (Design #2- Section B) is a more complex design, including an offset dual-polarized feed. In this case, more details on the antenna parameters/performances (i.e. F/D value, feed position, gain and aperture efficiency, etc.) are discussed.

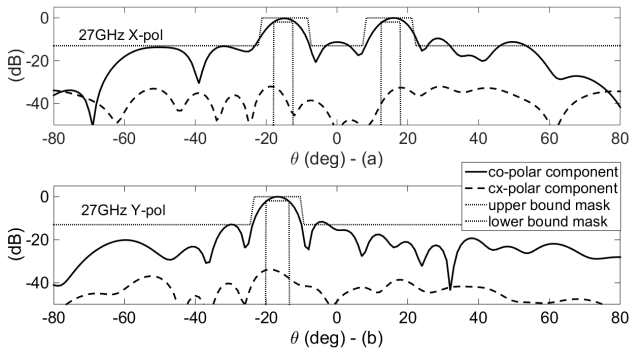

FIGURE 13. Full-wave simulation of the synthesized reflectarray patterns (H-plane, i.e. xz-plane in Fig. 1): (a) x-polarized component at 27 GHz; (b) y-polarized component at 27 GHz.

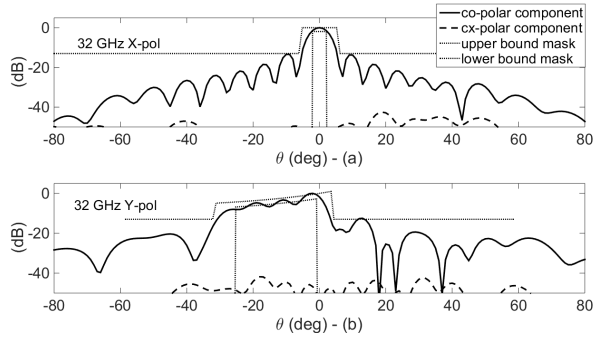

FIGURE 14. Full-wave simulation of the synthesized reflectarray patterns (H-plane, i.e. xz-plane in Fig. 1): (a) x-polarized component at 32 GHz; (b) y-polarized component at 32 GHz.

A. DESIGN #1

A 3 × 15-reflectarray prototype illuminated by a normally incident plane wave is synthesized to demonstrate the high versatility of the proposed unit cell in achieving arbitrary and independent beam directions and/or shapes (i.e. multi-beam or cosecant-beam patterns) at each frequency and each polarization. In particular, the coefficients over the reflectarray cells, and therefore the elements' scaling factors, are synthesized by imposing the following constraints: the x-polarized elements (i.e. L_{1x}, S_{1x}), working at 27 GHz, are chosen to achieve a dual-beam radiation pattern pointing towards the directions $\theta_{MB1} = -15°$ and $\theta_{MB2} = +15°$, in the H-plane (Fig. 13(a)); the y-polarized 27 GHz-elements (i.e. L_{1y}, S_{1y}), are synthesized to steer the main-lobe towards the direction $\theta_{MB} = -17.5°$, in the H-plane (Fig. 13(b)); whilst the elements working at 32 GHz are respectively chosen to point the main beam at $\theta_{MB} = 0°$ (x-polarized elements, i.e. L_{2x},S_{2x}) and to radiate a cosecant shaped pattern (y-polarized elements, i.e. L_{2y},S_{2y}), in the H-plane (Fig. 14). The full-wave simulations of the overall reflectarray structure are reported in Figs. 13 and 14. A normally incident plane-wave is considered (x-polarized for the case illustrated in Figs. 13(a) and 14(a); y-polarized for the case depicted in Figs. 13(b) and 14(b)). Quite low cross-polar components can be observed in Figs. 13, 14.

Finally, a very good agreement can be appreciated between the simulated radiation patterns and the imposed synthesis constraints (Figs. 13, 14), showing the effectiveness/versatility of the adopted dual-band/dual-polarized unit cell.

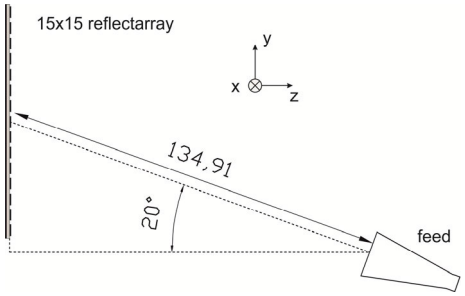

FIGURE 15. Schematic layout of the designed reflectarray prototype.

B. DESIGN #2

A 15 × 15 reflectarray is designed to independently steer the main lobes at the two different operating frequencies (i.e $\theta_{MB} = 20°$ at 27 GHz and $\theta_{MB} = 13°$ at 32 GHz, in the E-plane), for both polarizations.

The reflecting surface is illuminated by a dual-polarization horn (e.g. A-Info, LB-SJ-180400, 18-40 GHz Dual Polarization Horn Antenna) which is placed in the E-plane (i.e. the yz-plane in Fig. 15), at a distance of 135 mm from the reflecting surface, with an offset angle of about 20° (F/D≅1.2). The horn is characterized by a 15 dB-gain, with an average 3dB-beamwidth value respectively equal to 34°, at 27GHz, and to 30°, at 32GHz. The four fractal elements, embedded into each unit cell, are properly synthesized to compensate for the phase delay in the paths from the feed, as well as to introduce a proper phase contribution able to meet the imposed synthesis constraints [13], [32]. Figs. 16 and 17 show the computed radiation patterns of the synthesized antenna (continuous lines), in the E-plane (i.e. yz-plane in Fig. 15). It is possible to observe how a proper choice of the four sets of miniaturized patches allows to focalize the patterns along the desired directions at each considered frequency and polarization. Furthermore, very low cross-polarization levels can be observed in the same figures (dashed lines).

To highlight the effectiveness of the proposed reflectarray in achieving a well-defined set of focalized beams, Figs. 16 and 17 show the comparison with the uncompensated patterns (dotted lines), namely the patterns that would be radiated by an array of 15 × 15 identical cells, illuminated by the same feed. As it is well known, this array could not be able to compensate for the phase delay in the paths from the feed, thus being unable to focus the beam along the desired directions, as compared to the synthesized reflectarray.

Fig. 18 illustrates the gain patterns vs frequency, computed respectively along $\theta_{MB} = 20°$, in the case of the 27 GHz-radiation pattern, and along $\theta_{MB} = 13°$, in the case of the 32GHz-radiation pattern.

A greater gain peak value (≅ 25.7dB) can be observed for the 32GHz-pattern (i.e. the gain difference between the two operating frequencies is about 2.8 dB), mainly due to the greater electrical size and the lower spillover,

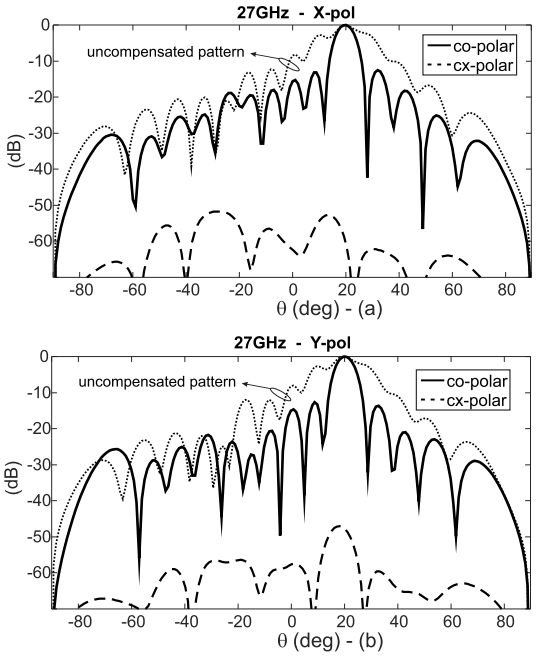

FIGURE 16. Computed radiation patterns (E-plane, i.e. yz-plane in Fig. 15): (a) x-polarized component at 27 GHz (co-polar, cross-polar and uncompensated patterns); (b) y-polarized component at 27 GHz (co-polar, cross-polar and uncompensated patterns).

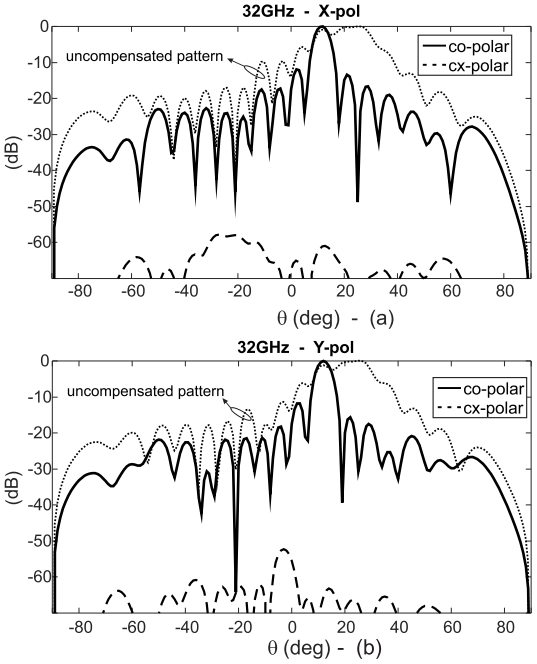

FIGURE 17. Computed radiation patterns (E-plane, i.e. yz-plane in Fig. 15): (a) x-polarized component at 32 GHz (co-polar, cross-polar and uncompensated patterns); (b) y-polarized component at 32 GHz (co-polar, cross-polar and uncompensated patterns).

characterizing the antenna aperture at the higher operating frequency (32 GHz). Furthermore, the simulated gain patterns show a 1dB gain bandwidth approximately equal to 2.4% at both operating frequencies.

The antenna efficiency, obtained as the ratio between the computed gain and the maximum directivity ($D = 4\pi A/\lambda^2$),

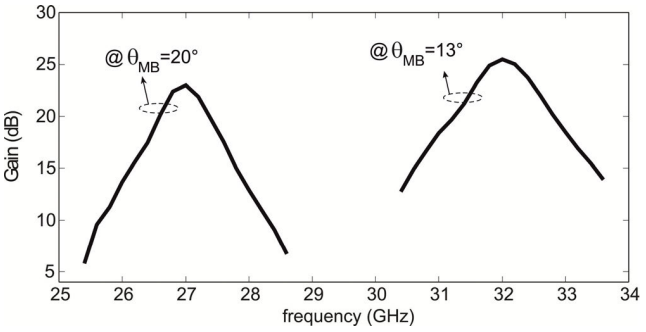

FIGURE 18. Simulated gain pattern versus frequency in the E-plane (i.e. yz-plane in Fig. 1): y-polarized component.

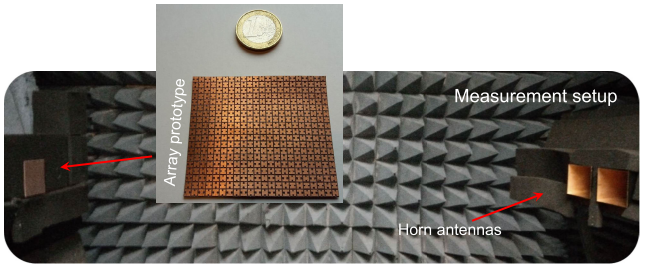

FIGURE 19. Reflection phase measurement setup and the dual-band/dual-polarized array prototype.

A being the area of the reflectarray surface, is relatively small. As a matter of fact, the small size of the reflecting surface, in conjunction with the large feed beam-width, causes very high spillover losses, giving an aperture efficiency equal to the following values: 29% (at 27 GHz) and 38% (at 32 GHz). Anyway, it is important to stress how the reflectarray prototype is designed for the unique purpose of demonstrating the effectiveness of the proposed configuration in offering an independent control of antenna radiation features, at both considered frequencies and polarizations. For this reason, the other antenna performances (i.e. efficiency, bandwidth, etc.) are not properly optimized at this stage.

IV. EXPERIMENTAL VALIDATION OF THE UNIT CELL

In order to give a preliminary experimental validation of the proposed dual-band/dual-polarized unit cell, a small array prototype is realized and tested in the Microwave Laboratory of the University of Calabria (Fig. 19). The array is printed on a Diclad880 substrate, having $\varepsilon_r = 2.24$ and $h = 0.254$mm. A periodicity equal to 5.5 mm is fixed in both directions. The patches embedded in each unit cell are characterized by the following dimensions: $L_{1x} = L_{1y} = 2.485$ mm – $S_{1x} = S_{1y} = 0.31$, $L_{2x} = L_{2y} = 2.32$ mm – $S_{2x} = S_{2y} = 0.25$, giving a minimum distance between two adjacent patches equal to 0.3 mm. The cell operates in a dual band mode in correspondence of about 28 GHz and 33 GHz, in both x and y polarizations.

Two identical transmitting and receiving standard horn antennas (operating within the [26.5÷40] GHz frequency band), are adopted to detect the field reflected by the array along the broadside direction in the far-field region [9], for both polarizations. The reflection phase curve of the cell is

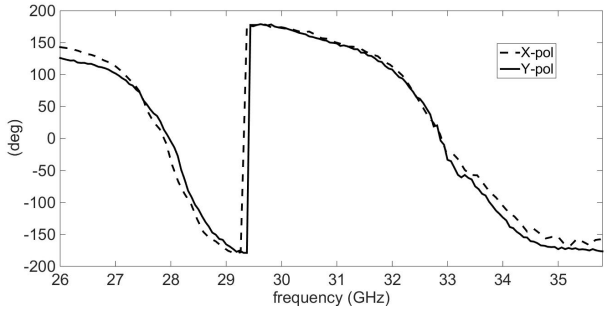

FIGURE 20. Measured phase curves vs frequency for different polarizations.

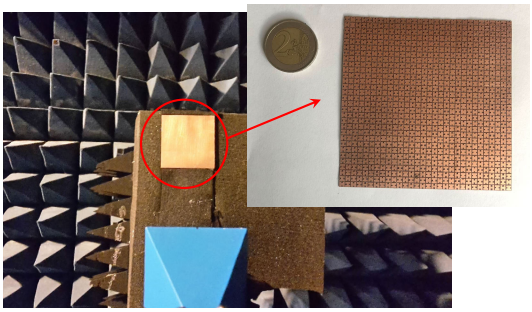

FIGURE 21. Photograph of the dual-band/dual-polarized reflectarray prototype.

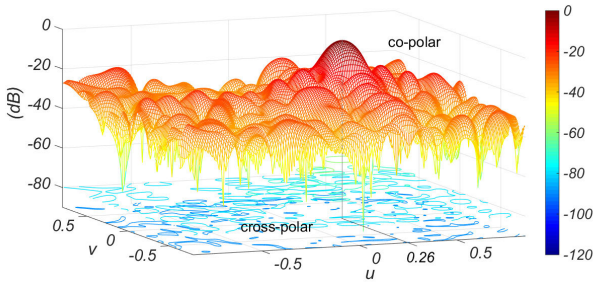

FIGURE 22. Simulated 3D patterns for Y-polarization at $f_1 = 28.7$GHz.

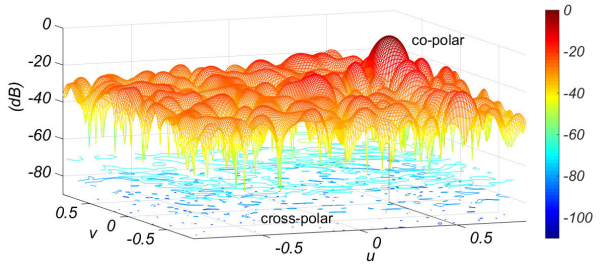

FIGURE 23. Simulated 3D patterns for Y-polarization at $f_1 = 32.8$GHz.

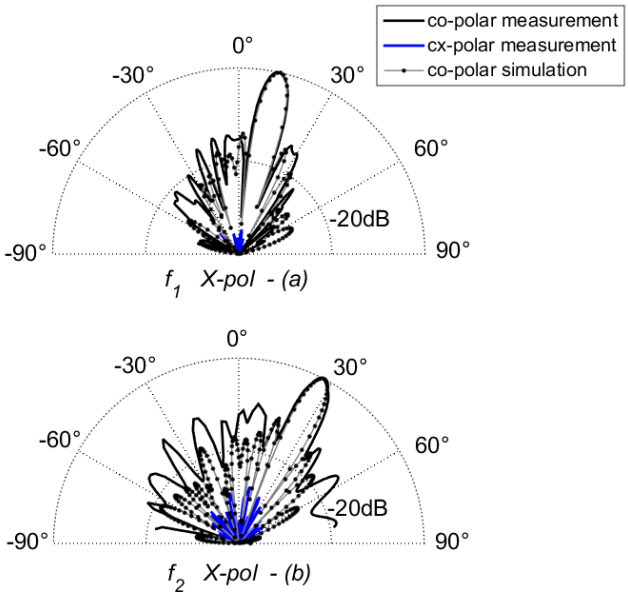

FIGURE 24. Measured and simulated radiation patterns for X-polarization at (a) $f_1 = 28.7$GHz; (b) $f_2 = 32.8$GHz.

measured within the frequency range 26.5÷36 GHz (Fig. 20). A full phase variation around both operating frequencies, for both polarizations, can be observed.

A small frequency shift can be identified between the two different polarizations, mainly due to the manufacturing errors tolerance related to the adopted printed circuit board (PCB) milling process [34], as well as to possible misalignments between the prototype and the horn antennas system. Anyway, the effects due to the above errors can be reduced by adopting a more precise fabrication process, as that described in [30], [35]. In conclusion, it can be stated that the experimental results confirm the dual band/dual-polarized behavior of the proposed configuration.

V. DESIGN AND TEST OF DUAL-BAND DUAL-LINEAR POLARIZATION REFLECTARRAY

In order to test the ability of the proposed cell in producing independent beams at two different frequencies and polarizations, a 15 × 15 reflectarray prototype (Fig. 21) is designed and experimentally tested. Figures 22 and 23 show the 3D plot of the synthesized patterns in u-v coordinates, where $u = \sin\theta\cos\phi$ and $v = \sin\theta\sin\phi$. In order to avoid the feed blockage effects in measurements, the main beam deviation is performed along the H-plane (i.e. the xz-plane in Fig. 15, namely $\phi = 0°$), normal to the plane containing the feed (i.e. yz-plane in Fig. 15). As depicted in Figs. 22 and 23, the antenna is designed to point its main beams along the direction equal to 15°, in the H-plane, at the first frequency $f_1 = 28.7$GHz (see the co-polar pattern in Fig. 22), and along the direction equal to 30° at the second frequency $f_2 = 32.8$ GHz (see the co-polar pattern in Fig. 23). The aforementioned synthesis constraints are imposed for both X and Y polarization components. Very low cross-polar components can be appreciated at both frequencies, for all directions of observation (Figs. 22-23).

In order to prove the effectiveness of the proposed design, a far-field facility is adopted to test the antenna. In Figs. 24 and 25, the measured co-polar patterns are successfully compared to the simulated results. A very small shift in the main beam positions and some higher side lobes can be observed. These latter are mainly due to possible manufacturing errors and misalignments in the adopted measurement system. The measured cross-polar components are also

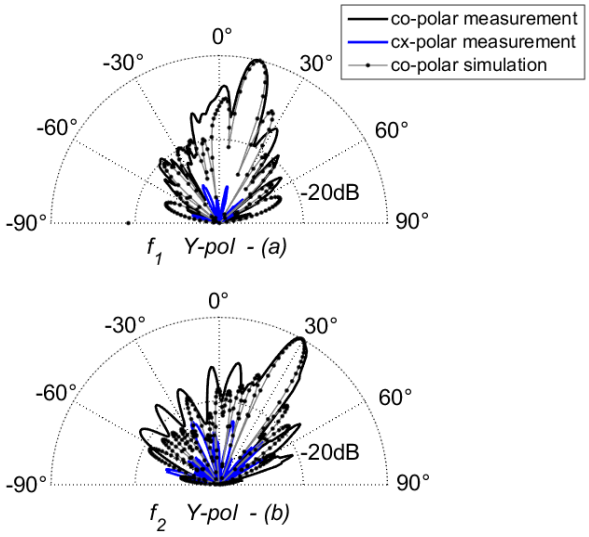

FIGURE 25. Measured and simulated radiation patterns for Y-polarization at (a) $f_1 = 28.7$GHz; (b) $f_2 = 32.8$GHz.

reported in the same figures, showing very lower intensity levels (about −30dB) with respect to the co-polar field.

In conclusion, the achieved experimental results provide a satisfactory preliminary validation of the proposed configuration, which can be considered very promising for dual-band dual-polarization applications.

VI. CONCLUSION

A novel dual-polarized reflectarray cell has been introduced to cover two different frequency bands centered at 27 and 32 GHz. The proposed configuration provides very small cell sizes and a very thin single layer structure. A thoroughly parametric analysis of the unit cell has been performed, demonstrating the independence between the designed frequency bands and polarizations. The proposed compact cell has been successful adopted to demonstrate reflectarrays capabilities in achieving arbitrary beam directions/shapes, under the dual-band/dual polarization operation mode. A successful experimental validation of the proposed configuration has been performed and discussed. Due to its versatility, the proposed dual-band/dual-polarized reflectarray cell is strongly appealing for future 5G applications.

REFERENCES

[1] T. S. Rappaport, Y. Xing, G. R. MacCartney, A. F. Molisch, E. Mellios, and J. Zhang, "Overview of millimeter wave communications for fifth-generation (5G) wireless networks–with a focus on propagation models," *IEEE Trans. Antennas Propag.*, vol. 65, no. 12, pp. 6213–6230, Dec. 2017.

[2] T. S. Rappaport, S. Sun, R. Mayzus, H. Zhao, Y. Azar, K. Wang, G. N. Wong, J. K. Schulz, M. Samimi, and F. Gutierrez, "Millimeter wave mobile communications for 5G cellular: It will work!," *IEEE Access*, vol. 1, pp. 335–349, 2013.

[3] I. F. Akyildiz, S. Nie, S.-C. Lin, and M. Chandrasekaran, "5G roadmap: 10 key enabling technologies," *Comput. Netw.*, vol. 106, pp. 17–48, Sep. 2016.

[4] W. Hong, Z. H. Jiang, C. Yu, J. Zhou, P. Chen, Z. Yu, H. Zhang, B. Yang, X. Pang, M. Jiang, Y. Cheng, M. K. T. Al-Nuaimi, Y. Zhang, J. Chen, and S. He, "Multibeam antenna technologies for 5G wireless communications," *IEEE Trans. Antennas Propag.*, vol. 65, no. 12, pp. 6231–6249, Dec. 2017.

[5] O. M. Haraz, A. Elboushi, S. A. Alshebeili, and A.-R. Sebak, "Dense dielectric patch array antenna with improved radiation characteristics using EBG ground structure and dielectric superstrate for future 5G cellular networks," *IEEE Access*, vol. 2, pp. 909–913, 2014.

[6] W. T. Sethi, M. A. Ashraf, A. Ragheb, A. Alasaad, and S. A. Alshebeili, "Demonstration of millimeter wave 5G setup employing high-gain vivaldi array," *Int. J. Antennas Propag.*, vol. 2018, May 2018, Art. no. 3927153.

[7] J. Huang and J. Encinar, *Reflectarray Antennas*. Hoboken, NJ, USA: Wiley, 2008.

[8] M. H. Dahri, M. H. Jamaluddin, M. I. Abbasi, and M. R. Kamarudin, "A review of wideband reflectarray antennas for 5G communication systems," *IEEE Access*, vol. 5, pp. 17803–17815, 2017.

[9] D. M. Pozar and T. A. Metzler, "Analysis of a reflectarray antenna using microstrip patches of variable size," *Electron. Lett.*, vol. 29, no. 8, pp. 657–658, 1993.

[10] J. Huang and R. J. Pogorzelski, "A ka-band microstrip reflectarray with elements having variable rotation angles," *IEEE Trans. Antennas Propag.*, vol. 46, no. 5, pp. 650–656, May 1998.

[11] J. A. Encinar and J. A. Zornoza, "Broadband design of three-layer printed reflectarrays," *IEEE Trans. Antennas Propag.*, vol. 51, no. 7, pp. 1662–1664, Jul. 2003.

[12] E. Carrasco, M. Barba, and J. A. Encinar, "Reflectarray element based on aperture-coupled patches with slots and lines of variable length," *IEEE Trans. Antennas Propag.*, vol. 55, no. 3, pp. 820–825, Mar. 2007.

[13] F. Venneri, S. Costanzo, and G. Di Massa, "Design and validation of a reconfigurable single varactor-tuned reflectarray," *IEEE Trans. Antennas Propag.*, vol. 61, no. 2, pp. 635–645, Feb. 2013.

[14] S. V. Hum and J. Perruisseau-Carrier, "Reconfigurable reflectarrays and array lenses for dynamic antenna beam control: A review," *IEEE Trans. Antennas Propag.*, vol. 62, no. 1, pp. 183–198, Jan. 2014.

[15] P. Nayeri, F. Yang, and A. Z. Elsherbeni, "Beam-scanning reflectarray antennas: A technical overview and state of the art.," *IEEE Antennas Propag. Mag.*, vol. 57, no. 4, pp. 32–47, Aug. 2015.

[16] S. Costanzo, F. Venneri, A. Raffo, G. Di Massa, and P. Corsonello, "Radial-shaped single varactor-tuned phasing line for active reflectarrays," *IEEE Trans. Antennas Propag.*, vol. 64, no. 7, pp. 3254–3259, Jul. 2016.

[17] S. Costanzo, F. Venneri, G. Di Massa, A. Borgia, and A. Raffo, "Bandwidth performances of reconfigurable reflectarrays: State of art and future challenges," *Radioengineering*, vol. 27, no. 1, pp. 1–9, Apr. 2018.

[18] S. Costanzo, F. Venneri, A. Raffo, and G. Di Massa, "Dual-layer single-varactor driven reflectarray cell for broad-band beam-steering and frequency tunable applications," *IEEE Access*, vol. 6, pp. 71793–71800, 2018.

[19] E. Martinez-de-Rioja, J. A. Encinar, M. Barba, R. Florencio, R. R. Boix, and V. Losada, "Dual polarized reflectarray transmit antenna for operation in Ku- and ka-bands with independent feeds," *IEEE Trans. Antennas Propag.*, vol. 65, no. 6, pp. 3241–3246, Jun. 2017.

[20] Y. Pan, Y. R. Zhang, and X. Yu, "A X/Ku dual-band reflectarray design with cosecant squared shaped beam," *Microw. Opt. Technol. Lett.*, vol. 56, no. 9, pp. 2028–2034, Sep. 2014.

[21] Z. Hamzavi-Zarghani and Z. Atlasbaf, "A new broadband single-layer dual-band reflectarray antenna in X- and ku-bands," *IEEE Antennas Wireless Propag. Lett.*, vol. 14, pp. 602–605, 2015.

[22] R. S. Malfajani and Z. Atlasbaf, "Design and implementation of a dual-band single layer reflectarray in x and k bands," *IEEE Trans. Antennas Propag.*, vol. 62, no. 8, pp. 4425–4431, Aug. 2014.

[23] M. H. Dahri, M. H. Jamaluddin, M. Khalily, M. I. Abbasi, R. Selvaraju, and M. R. Kamarudin, "Polarization diversity and adaptive beamsteering for 5G reflectarrays: A review," *IEEE Access*, vol. 6, pp. 19451–19464, 2018.

[24] S. Costanzo, F. Venneri, A. Borgia, and G. Di Massa, "A single-layer dual-band reflectarray cell for 5G communication systems," *Int. J. Antennas Propag.*, vol. 2019, pp. 1–9, Mar. 2019.

[25] S. Costanzo, F. Venneri, and G. Di Massa, "A single layer dual band/dual polarized reflectarray cell for 5G," in *Proc. 13th Eur. Conf. Antennas Propag.*, Krakow, Poland, Mar. 2019, pp. 1–3.

[26] S. Costanzo, F. Venneri, and G. Di Massa, "Modified minkowski fractal unit cell for reflectarrays with low sensitivity to mutual coupling effects," *Int. J. Antennas Propag.*, vol. 2019, Feb. 2019, Art. no. 4890710.

[27] S. Costanzo and F. Venneri, "Miniaturized fractal reflectarray element using fixed-size patch," *IEEE Antennas Wireless Propag. Lett.*, vol. 13, pp. 1437–1440, 2014.

[28] K. H. Sayidmarie and M. E. Bialkowski, "Fractal unit cells of increased phasing range and low slopes for single-layer microstrip reflectarrays," *IET Microw., Antennas Propag.*, vol. 5, no. 11, pp. 1371–1379, 2011.
[29] S. Costanzo, F. Venneri, G. Di Massa, A. Borgia, A. Costanzo, and A. Raffo, "Fractal reflectarray antennas: State of art and new opportunities," *Int. J. Antennas Propag.*, vol. 2016, Dec. 2016, Art. no. 7165143.
[30] S. Costanzo, I. Venneri, G. Di Massa, and A. Borgia, "Benzocyclobutene as substrate material for planar millimeter-wave structures: Dielectric characterization and application," *J. Infrared Millim. THz Waves*, vol. 31, no. 1, pp. 66–77, 2010.
[31] M. J. Marcus, "WRC-19 issues: A survey," *IEEE Wireless Commun.*, vol. 24, no. 1, pp. 2–3, Feb. 2017.
[32] *Ansoft Designer*. [Online]. Available: https://www.ansys.com
[33] F. Venneri, S. Costanzo, G. Di Massa, and G. Angiulli, "An improved synthesis algorithm for reflectarrays design," *IEEE Antennas Wireless Propag. Lett.*, vol. 4, pp. 258–261, 2005.
[34] *LPKF ProtoMat*. [Online]. Available: https://www.lpkf.com/
[35] S. Costanzo, F. Venneri, A. Borgia, I. Venneri, and G. Di Massa, "60 GHz microstrip reflectarray on a benzocyclobutene dielectric substrate," *IET Sci., Meas. Technol.*, vol. 5, no. 4, pp. 134–139, 2011.

SANDRA COSTANZO (Senior Member, IEEE) received the Laurea *(summa cum laude)* degree in computer engineering from the Università della Calabria, Italy, in 1996, and the Ph.D. degree in electronic engineering from the Mediterranea University of Reggio Calabria, Italy, in 2000. In 2017, she awarded the Italian National Scientific Qualification for the Full Professor position. Since 2019, she is currently an Associate with IREA-CNR, Naples. In the framework of the European School of Antennas, she was a Teacher with the Antenna Centre of Excellence course Phased Arrays and Reflectarray, held at The Netherlands Organization for Applied Scientific Research, The Netherlands, in 2005. Since 1996, she has been involved in many research projects funded by international and national companies. She is also an Associate Professor with the Università della Calabria, where she is the Coordinator of Master's degree in telecommunication engineering. She teaches courses on electromagnetic waves propagation, antennas, remote sensing, radar and electromagnetic diagnostics. She has authored or coauthored over 160 contributions in international journals, books, and conferences. Her research interests include near-field/far-field techniques, antenna measurement techniques, antenna analysis and synthesis, numerical methods in electromagnetics, millimeter wave antennas, reflectarrays, synthesis methods for microwave structures, electromagnetic characterization of materials, biomedical applications, and radar technologies. She is a member of the IEEE MTT-28 Biological Effects and Medical Applications Committee, the IEEE South Italy Geoscience and Remote Sensing Chapter, Consorzio Nazionale Interuniversitario per le Telecomunicazioni (CNIT), Società Italiana di Elettromagnetismo (SIEM), Centro Interuniversitario sulle Interazioni fra Campi Elettromagnetici e Biosistemi (ICEMB), and Board Member of the IEEE AP/ED/MTT North Italy Chapter. She received the Telecom Prize for the Best Laurea Thesis, in 1996, and the Best Academia & Research Application in Aerospace and Defense 2013 Award for the application Software Defined Radar using the NI USRP 2920 platform. She is also an Associate Editor of IEEE Access, the IEEE Journal of Electromagnetics, RF, and *Microwaves in Medicine and Biology, Electronics (section 'Microwave and Wireless Communications'), and an Editorial Board Member of Radioengineering and International Journal of RF and Microwave Computer-Aided Engineering. She is the Editor of the books Microwave Materials Characterization (INTECH, 2012) and Wave Propagation Concepts for Near-Future Telecommunication Systems (INTECH, 2017). She was a Lead Editor of Special Issues titledReflectarray Antennas: Analysis and Synthesis Techniques (2012), Advances in Radar Technologies (2013), Compressed Sensing: Applications in Radar and Communications (2016), Bioengineering Applications of Electromagnetic Wave Propagation (2019), and Microwave Sensors for Biomedical Applications (2020).*

FRANCESCA VENNERI (Member, IEEE) received the degree in information technology engineering from the University of Calabria, Italy, in 1998, and the Ph.D. degree in electronic engineering from the University Mediterranea of Reggio Calabria, in 2002. She is currently an Assistant Professor with the University of Calabria. Her research interests include microstrip reflectarrays, antenna analysis and synthesis, RFID technology, metamaterial absorbers. She is member of the IEEE Antennas and Propagation Society, the Società Italiana di Elettromagnetismo (SIEm), and the Consorzio Consorzio Nazionale Interuniversitario per le Telecomunicazioni (CNIT).

ANTONIO BORGIA (Member, IEEE) was born in Reggio Calabria, Italy. He received the Laurea degree in computer engineering and the Ph.D. degree in system and computer engineering from the University of Calabria, in 2008 and 2013, respectively. He is a member of Consorzio Nazionale Interuniversitario per le Telecomunicazioni (CNIT), Centro Nazionale di Ricerca Interuniversitario sulla Interazione fra Campi Elettromagnetici e Biosistemi (ICEmB), and Società Italiana di Elettromagnetismo (SIEm). He has (co)authored more than 50 contributions in international journals and conferences. His research interests isnclude millimeter-wave antennas and technologies, printed antennas, and reflectarrays.

GIUSEPPE DI MASSA (Life Senior Member, IEEE) was born in Barano d'Ischia, Naples, Italy, in 1948. He received the Laurea degree in electronic engineering from the Università di Napoli Federico II, Naples, in 1973. From 1978 to 1979, he was a Professor of antennas with the Università di Napoli Federico II. In 1980, he joined the Università della Calabria, Italy, as a Professor of electromagnetic waves. Since 1985, he has been an Associate Professor, and since 1994, a Full Professor, with the Università della Calabria, where he teaches antennas and electromagnetic fields. From 1985 to 1986, he was a Scientific Associate with CERN, Geneva. In 1988, he was a Visiting Professor with the Brookhaven National Laboratory, Long Island, NY, USA. From 1997 to 2002, he was the Dean of the Department of Elettronica, Informatica and Sistemistica and the President of Programming Committee with the Università della Calabria. From 2000 to 2017, he was the Chairman of the Telecommunication Engineering Program with the Università della Calabria. He has authored/coauthored over 350 scientific articles, mainly on international scientific journals or proceedings of international conferences. He is the Principal Investigator or Coordinator of many research programs, granted by national and international research organizations, as well as by leading national companies. His main research interests include applied computational electromagnetics, microstrip antennas, microwave integrated circuits, reflectarrays, Gaussian beam solutions, millimeter wave antennas, near-field measurements, electromagnetic characterization of materials, and innovative radar antennas and technologies. He was the Italian Delegate in the European COST 284 Innovative Antennas for Emerging Terrestrial and Space-Based Applications, from 2002 to 2006, and from 2007 to 2011, in the COST Action IC0603: Antenna Systems and Sensors for Information Society Technologies. From 2003 to 2007, he participated in the Network of Excellence Antenna Centre of Excellence, where he was the part of the Governing Board and the Leader of Work Group WP 1.2-1: Antenna Measurement Services. From 2011 to 2014, he was the Italian Delegate in the Management Committee of the COST Action IC1102, Versatile Integrated, and Signal-Aware Technologies for Antennas. Since 2019, he his Emeritus Professor at Università della Calabria.